A Simple Synthesis of an N-Doped Carbon ORR Catalyst: Hierarchical Micro/Meso/Macro Porosity and Graphitic Shells

Eisenberg, D.; Stroek, W.; Geels, N.J.; Sandu, C.S.; Heller, A.; Yan, N.; Rothenberg, G.

DOI
10.1002/chem.201504568

Publication date
2016

Document Version
Final published version

Published in
Chemistry - A European Journal

ChemPubSoc Europe

DOI: 10.1002/chem.201504568

CHEMISTRY
A European Journal
Communication

Carbon Electrocatalysts

A Simple Synthesis of an N-Doped Carbon ORR Catalyst: Hierarchical Micro/Meso/Macro Porosity and Graphitic Shells

David Eisenberg,*[a] Wowa Stroek,[a] Norbert J. Geels,[a] Cosmin S. Sandu,[b] Adam Heller,[c] Ning Yan,*[a] and Gadi Rothenberg*[a]

Abstract: Replacing platinum as an oxygen reduction catalyst is an important scientific and technological challenge. Herein we report a simple synthesis of a complex carbon with very good oxygen reduction reaction (ORR) activity at pH 13. Pyrolysis of magnesium nitrilotriacetate yields a carbon with hierarchical micro/meso/macro porosity, resulting from in situ templating by spontaneously forming MgO nanoparticles and from etching by pyrolysis gases. The mesopores are lined with highly graphitic shells. The high ORR activity is attributed to a good balance between high specific surface area and mass transport through the hierarchical porosity, and to improved electronic conductivity through the graphitic shells. This novel carbon has a high surface area (1320 m^2g^{-1}), and high nitrogen content for a single precursor synthesis (~6%). Importantly, its synthesis is both cheap and easily scalable.

Oxygen reduction is a key reaction in a wide range of applications,[1–3] such as fuel cells, metal–air batteries, and biological sensors. Most of today's oxygen cathodes are based on platinum catalysts. In theory, such fuel cells could power cars for mass transportation,[4] but there is a catch: there is simply not enough platinum to go around. The car industry already consumes over 60% of the annual world platinum supply in catalytic converters.[5] Fuel-cell powered cars may require ~5 times as much precious metal.[6,7] Thus, any practical scenario must include the replacement of platinum with a more abundant (and cheaper!) alternative.

Research in catalysis and materials science offers several alternatives to platinum,[8] including alloys,[9,10] metal oxides,[11,12] and metal-free materials[13] such as nitrogen-doped carbon.[14–18] This last option is especially appealing, because nitrogen and carbon are ubiquitous on Earth, and their continued supply is guaranteed. Carbon, one of the oldest low-value energy sources known to mankind,[19] is making a comeback into energy research as a high-value material. It is hailed as a key component for tomorrow's electrocatalysts,[13] supercapacitors,[20] and battery electrodes.[21]

Carbon electrocatalysts must meet four key conditions. The first three represent the classic electrochemical constraints: Active sites allowing a fast and selective oxygen reduction; electron conduction; and an open microstructure permitting efficient mass transport of O_2 and OH^- to and from the active sites. However, the carbon in question must also be made cheaply and simply in ton quantities.[6,22,23] It is this combination of economic and scientific constraints that makes the search for platinum alternatives such an exciting challenge.

We now report the discovery of a simple route to nitrogen-doped carbon with hierarchical micro/meso/macro porosity that is an excellent oxygen reduction catalyst.[13–18] Its synthesis is based on the pyrolysis of magnesium nitrilotriacetate, yielding a carbon with half the surface area of graphene and a high nitrogen content (1320 m^2g^{-1} and 6 wt%, respectively). Remarkably, the mesopores are lined with highly graphitic carbon shells, and the pores are interconnected. This creates a structure with the unusual combination of both rapid mass transfer and good electronic conductivity.

Mixing magnesium carbonate and nitrilotriacetic acid in hot water yields magnesium nitrilotriacetate in less than a minute (Figure 1).[24] The salt was precipitated with ethanol, giving $HMgN(CH_2COO)_3{\cdot}3(H_2O)$ (herein MgNTA). Batches of 25 g were prepared routinely in each synthesis. Pyrolysis of MgNTA in argon at 900 °C for one hour yielded a fine black powder. TEM

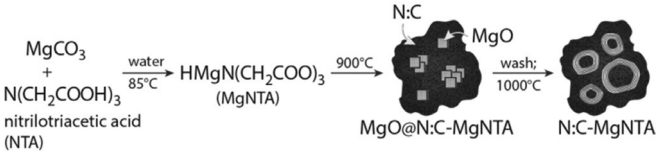

Figure 1. Schematic synthesis of a nitrogen-doped porous carbon with hierarchical porosity and graphitic shells.

[a] Dr. D. Eisenberg, W. Stroek, Ing. N. J. Geels, Dr. N. Yan, Prof. Dr. G. Rothenberg
Van 't Hoff Institute for Molecular Sciences
University of Amsterdam, Science Park 904
1098 XH Amsterdam (The Netherlands)
E-mail: d.eisenberg@uva.nl
n.yan@uva.nl
g.rothenberg@uva.nl
Homepage: http://hims.uva.nl/hcsc

[b] Dr. C. S. Sandu
3D-OXIDES, 70 Rue Gustave Eiffel
Saint Genis Pouilly, 01630 (France)

[c] Prof. Dr. A. Heller
McKetta Department of Chemical Engineering
University of Texas at Austin, 200 E. Dean Keeton St. Stop C0400
Austin, TX 78712 (USA)

Supporting information and ORCID(s) for this article is available on the WWW under http://dx.doi.org/10.1002/chem.201504568.

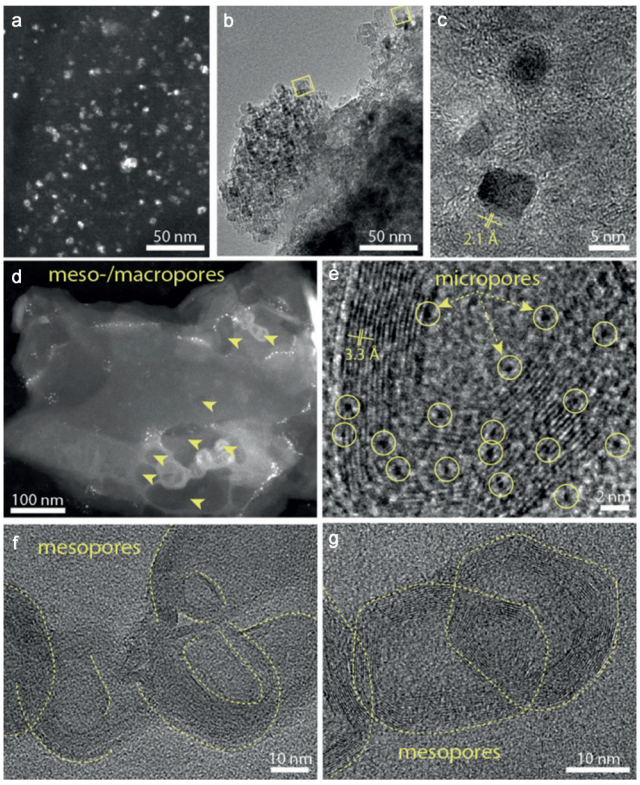

Figure 2. Transmission electron micrographs of carbons derived from MgNTA, wherein (a–c) refer to MgO@N:C-MgNTA after pyrolysis and (d–g) to the final N:C-MgNtA, after washing and annealing. a) dark-field image; b) bright-field image, with squares marking some cube-shaped MgO nanoparticles; c) high-resolution image, with spacing of MgO crystallite; d) low magnification STEM with several interconnected meso- and macropores marked by arrows; e) HRTEM image of a mesopores coated with a graphitic shell from panel (d), with spacing of shell, and circles marking some of the micropores; f–g) HRTEM of closed and open, interconnected and overlapping mesopores. See the Supporting Information for nonmarked versions of these images and additional TEM micrographs.

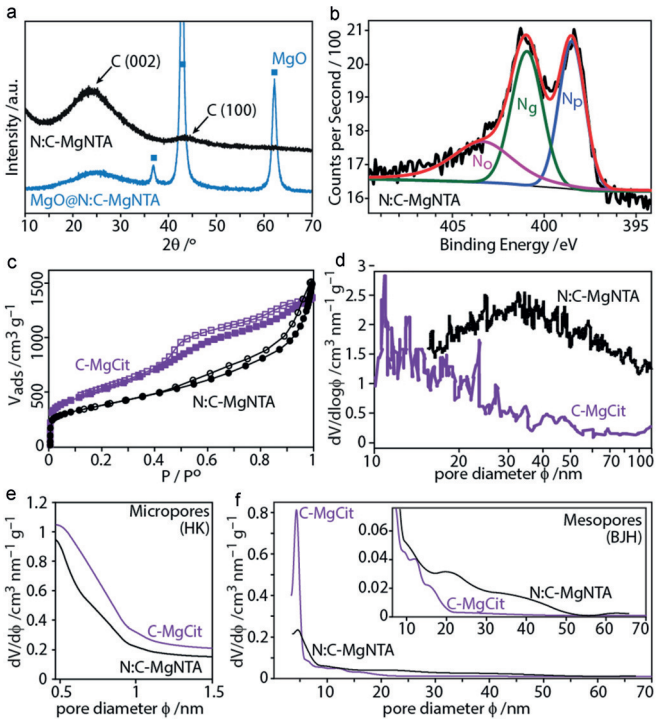

Figure 3. a) Powder X-ray diffraction of MgO@N:C-MgNTA (below, blue) and the final N:C-MgNTA (above, black), with MgO diffraction peaks marked by squares; b) X-ray photoelectron spectrum in the N 1s region of N:C-MgNTA, fitted by pyridinic (N_p), graphitic (N_g), and oxidized (N_O) functionalities; c) Nitrogen-adsorption isotherm on N:C-MgNTA and C-MgCit; d) Pore-size distribution (PSD) in N:C-MgNTA obtained by mercury intrusion porosimetry. PSDs calculated from the desorption isotherm: e) micropore region by the Horváth–Kawazoe method; f) mesopore region (enlarged in inset) by the Barrett–Joyner–Halenda method.

revealed an abundance of nanoparticles dispersed in the carbon matrix (Figure 2a–c and Figure S1, Supporting Information), in both separate and agglomerated form. These particles are cubic, with an average size of 6.4 ± 1.4 nm. They are agglomerated in clusters ranging in size over 10–100 nm. Chemical mapping by energy-dispersive X-ray spectroscopy showed that these particles are rich in magnesium (Figure S2, Supporting Information), and HRTEM of single particles (such as the one in Figure 2c) identifies *d*-spacing of 2.11 ± 0.02 Å, the same as in MgO (200).[25] Powder XRD (Figure 3a) exhibited a peak at $2\theta = 25^\circ$, assigned to the graphite (002) plane,[25] and three strong peaks at 37.0, 42.8, and 62.2°, corresponding to the (111), (200), and (220) faces of MgO.[25] Thus, the carbon matrix is rich with both separate and agglomerated magnesium oxide nanoparticles.

The MgO-containing carbon was washed with dilute citric acid (0.5 M), dissolving the MgO phase (cf. the disappearance of XRD peaks of MgO in Figure 3a and Figure S3, Supporting Information). The carbon was further annealed in argon at 1000 °C for one hour, following the protocol of Inagaki et al. This annealing promotes graphitization, as observed in the increased intensity of the graphite (002) and (100) XRD peaks in Figure 3a and Figure S3, Supporting Information. The yield of the carbon was about 3 g in each batch.

The TEM of the nitrogen-doped carbon derived from MgNTA ('N:C-MgNTA') reveals a unique morphology (Figure 2d–g). First, the carbon is microporous, exhibiting a wormlike structure typically identified as microporosity.[26] The observed holes have diameters of 0.3–0.6 nm (marked by circles in Figure 2e and Figure S4, Supporting Information); some appear close to shell walls and thus probably permeate the wall structure, which is just out of focus due to the limited depth of field. Second, there are many overlapping mesopores and macropores ranging in size from 5 to 100 nm (Figure 2d,f,g and Figures S5–S11, Supporting Information). High resolution TEM reveals that the pores are lined with highly ordered graphite, with 0.33 nm interlayer spacing, similar to graphite (002)[25] (Figure 2e). The graphitic shells are abundant, and many of them overlap (Figure 2f,g and Figures S3–S10, Supporting Information), which suggests percolation for 1) graphitic shells, possibly leading to improved conductivity in the material[27,28] and 2) pore interiors, possibly improving mass transport through the pore network. Some cavities have angular shapes and inner diameters of 6–7 nm (e.g. Figure 2e,g), correspond-

ing in size and shape to MgO nanoparticles. The rest of the shells have inner diameters of 10–100 nm, matching the size distribution of MgO agglomerates. Thus, crystallites and agglomerates of MgO serve a dual role: they are both in situ templates for creating mesopores and macropores, and also catalysts for the formation of graphitic shells. Graphene shells are known to form on MgO during CVD synthesis by interfacing with MgO crystal facets,[29,30] but they are usually thin (1–10 graphitic layers) and disordered. The observed graphitic shells are thicker (15 ± 5 graphitic layers, ~3–7 nm) and highly regular, which suggests that high-temperature annealing promotes graphitization on MgO cores.[31]

The pore structure and accessibility of N:C-MgNTA was studied by nitrogen adsorption and mercury intrusion porosimetry (Figure 3 c,d), and then compared with that of an undoped carbon prepared by the same method from magnesium citrate ('C-MgCit').[32] High-specific surface areas were observed in both carbons: 1320 m^2g^{-1} for N:C-MgNTA and 1840 m^2g^{-1} for C-MgCit. The nitrogen-adsorption isotherms (Figure 3 c) exhibited similarly steep rises at low relative pressures, which indicated the presence of micropores in both carbons. Analysis of this region of the isotherm by the micropore-specific Horváth–Kawazoe (HK) model revealed pore diameters of 0.5–1.0 nm.[33] While mesopores and macropores are templated by spontaneously forming MgO particles, microporosity evolves by in situ activation with gaseous products of pyrolysis.[34] Indeed, we identified the release of CO_2 and hydrocarbons at temperatures of 370–580 °C by mass spectrometry coupled to thermal gravimetric analysis (Figure S12, Supporting Information). Note that N:C-MgNTA differs from "ordinary" activated carbon by having two distinct pore-forming mechanisms, whereas mesopores in activated carbon arise from prolonged etching of micropores.

At higher relative pressures of nitrogen ($P/P^0>0.1$), a slope is observed in the isotherm, attributed to the filling of mesopores. Both carbons have small mesopores of 5 nm diameter (Figure 3 f). The pores are similar in size to those of the discrete MgO nanoparticles observed by TEM (e.g. Figure 2 a–c), which suggests that they are templated by these particles. This feature is not an artefact due to rapid monolayer evaporation, since it appears in calculations of both the adsorption and desorption branches. Carbon N:C-MgNTA is richer with large mesopores, whereas C-MgCit has more small mesopores (Figure 3 f). Furthermore, only the N:C-MgNTA isotherm rises steeply at high relative pressures, due to condensation in large mesopores and macropores. Presence of macropores and large mesopores was further confirmed by mercury intrusion porosimetry (Figure 3 d), which showed pores with 10–100 nm diameters in N:C-MgNTA. The micropores permeate the material (TEM Figure 2 e), and are thus accessible through the meso- and macropores. Thus, both electron microscopy and the N_2- and Hg- porosimetries point to a triple hierarchical micro/meso/macro pore structure in N:C-MgNTA.[16,18]

XPS of N:C-MgNTA shows peaks at 284, 400, and 531 eV (Figure S13, Supporting Information), corresponding to binding energies of C 1s, N 1s, and O 1s orbitals, respectively. Nitrogen is present at 5.7–5.8 wt% relative to the carbon, based on elemental analysis and XPS areas (see Table S1, Supporting Information). This level of N-doping is high, especially when originating from a single precursor, that is, without nitrogen from an external source.[14,16] The N 1s region in the XPS spectrum (Figure 3 b) fitted those of three typical and physically probable nitrogen moieties, revealing that 35% of nitrogen atoms are pyridinic, 37% are graphitic, and 28% are in oxidized environments. Both pyridinic and graphitic nitrogen atoms may provide catalytic sites for ORR,[35–38] and their high concentration in the carbon (4 wt% total) may be promising for catalysis.

The catalytic activity of the doped and undoped carbons towards ORR was investigated electrochemically in alkaline solution. Cyclic voltammetry in a N_2-saturated solution showed only capacitive currents (Figure 4 a), while saturating

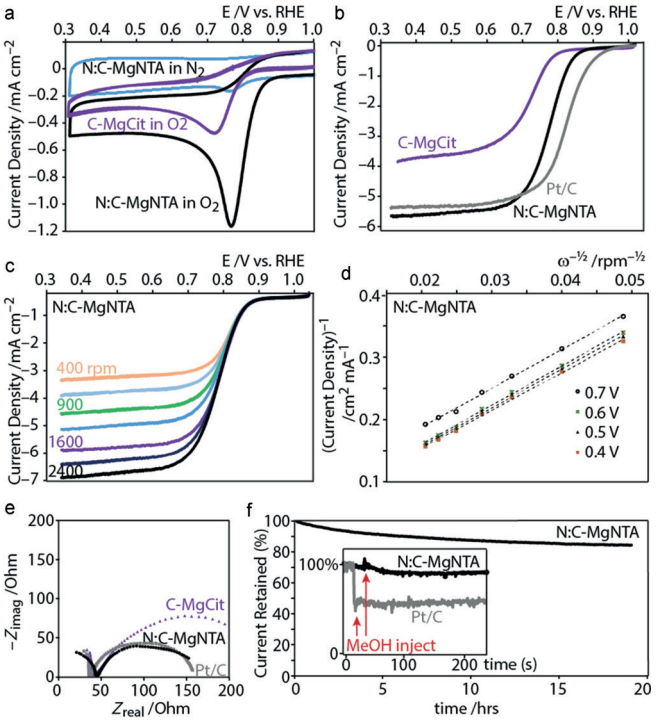

Figure 4. Electrocatalytic ORR on N:C-MgNTA and C-MgCit. a) Cyclic voltammetry in O_2- and N_2-saturated 0.1 M KOH solutions. b) Voltammetry in O_2-saturated solution at 1600 rpm rotation speed, compared to a commercial 20% wt Pt/C catalyst. c) LSV of N:C-MgNTA at different rotation rates (400, 600, 900, 1200, 1600, 2000, and 2400 rpm). All experiments were run at scan rates of 10 mV s^{-1}. d) Koutecký–Levich plot based on RDE data at several potentials vs. RHE. e) Nyquist plot obtained by potentiostatic electrochemical impedance spectroscopy at $E^{1/2}$. f) Chronoamperometric stability testing at $E=0.5$ V vs. RHE and 1600 rpm, while bubbling O_2; inset: chronoamperogram in which methanol (3 M) was injected.

the solution with O_2 led to pronounced reduction peaks for both carbons. The doped, hierarchically porous N:C-MgNTA was, however, a more active ORR catalyst than the undoped, macropore-free C-MgCit, despite the latter's higher surface area. Under mass-transport limiting conditions on a rotating disk electrode (RDE, 1600 rpm, Figure 4 b), the N:C-MgNTA exhibited an onset potential of 0.89 V vs. RHE, 60 mV positive of commercial 20 wt% Pt/C, and 70 mV more negative than un-

doped C-MgCit. The half-wave potential ($E^{1/2}$) for ORR on N:C-MgNTA is 0.75 vs. RHE. This value is ~100 mV more negative than the best-performing Pt/C and N-doped graphite/graphene ORR electrocatalysts in the literature (Table S2, Supporting Information). It falls within a ~200 mV range which defines the state-of-the-art in the literature.

To probe kinetics of ORR on the carbons, the rotation rate was varied in the voltammetric measurements (Figure 4c). Well-behaved limiting currents were observed, their onset potential constant, and their limiting current varying as expected from the Koutecký–Levich equation with the flux-defining angular velocity.[39] The Koutecký–Levich plots (Figure 4d and Figure S14, Supporting Information) are perfectly linear ($R^2 > 0.998$), indicative of first-order reaction kinetics towards dissolved O_2. The numbers of electrons transferred in the reaction, calculated from the Koutecký–Levich slopes,[39] are 4.28–4.34 electrons for N:C-MgNTA and 2.5–3.0 for C:MgCit. These values confirm that the nitrogen-doped carbon strongly prefers the $4e^-$ pathway, in contrast to the undoped carbon, which takes the $2e^-$ reduction pathway through H_2O_2.[35] The electron-transfer number exceeds 4, which may be due to the surface roughness of the carbon film. As recently shown by Hu et al.,[40] increased film roughness changes the reagent flow from laminar to turbulent, increasing local concentration of O_2 and the apparent electron-transfer number. The ORR activity of N:C-MgNTA was further established by potentiostatic electrochemical impedance spectroscopy (Figure 4e). The width of the semicircle, which corresponds to the catalyst charge-transfer resistance,[39] is similar for N:C-MgNTA and commercial Pt/C (121 Ohm and 127 Ohm, respectively), and nearly double (205 Ohm) for C-MgCit.

Chronoamperometry reveals the high durability of N:C-MgNTA (Figure 4f). The carbon retains 94% of the initial current density after 3 h and 80% of the current after 19 h, so its stability is superior to that of the commercial 20 wt% Pt/C electrodes.[15,16] The latter deteriorate by platinum particle agglomeration, dissolution, and surface poisoning.[2] We tested explicitly for poisoning by injecting methanol into the solution (Figure 4f, inset) during a chronoamperometric measurement. As expected, methanol promptly poisoned the platinum surface. Carbon N:C-MgNTA, on the other hand, did not show any current loss when methanol was injected.

We hypothesize that the excellent electrocatalytic activity of N:C-MgNTA stems from 1) its microstructure, balancing high specific surface area with many nitrogen active sites, against a hierarchical micro/meso/macro porosity, which enables facile mass transport of O_2 and OH^- to and from active sites and 2) the highly ordered graphitic shells which line the mesopores and boost conductivity. While C-MgCit has a larger surface area, the lack of nitrogen (known for its contribution to ORR catalysis)[35] and smaller proportion of meso- and macropores result in lower activity than that of N:C-MgNTA.

In summary, we report here the simple and scalable synthesis of an N-doped carbon with a unique microstructure. Like in the undoped analogue, spontaneously forming MgO nanoparticles provides in situ templates for mesopores and macropores, while pyrolysis gases etch micropores into the material, creating hierarchical micro/meso/macro porosity. The pores of the nitrogen-doped carbon are lined with nitrogen-enriched highly graphitic shells, deposited from the nitrogen and carbon content of the precursor salt. This carbon is an effective ORR catalyst, probably due to a combined effect of improved mass transport through the hierarchical porosity, and improved electrical conductivity through the network of graphitic shells. We believe that this material, with its simple synthesis protocol and easy scale-up, opens exciting avenues as a catalyst for ORR and for other electrochemical reactions.

Acknowledgements

We thank Dr. S. Mischler and P. Mettraux (EPFL, Switzerland) for XPS measurements, Prof. Nava Setter and the CIME-EPFL team for TEM investigation facilities, and Dr. C.B. Mullins, O. Mabayoje, W.G. Hardin, and J.T. Mefford (UT Austin) for help in the early stages of the project. A.H. thanks the Welch Foundation for Grant F-1131. This work is part of the Research Priority Area Sustainable Chemistry of the UvA, http://suschem.uva.nl.

Keywords: carbon shells · mesoporous materials · metal-free catalysts · microporous materials · oxygen reduction reaction

[1] *Handbook of Fuel Cells, Vol. 2* (Eds.: W. Vielstich, A. Lamm, H. A. Gasteiger), John Wiley & Sons, **2003**.
[2] Y. Nie, L. Li, Z. Wei, *Chem. Soc. Rev.* **2015**, *44*, 2168 – 2201.
[3] F. Cheng, J. Chen, *Chem. Soc. Rev.* **2012**, *41*, 2172 – 2192.
[4] M. K. Debe, *Nature* **2012**, *486*, 43 – 51.
[5] http://www.platinum.matthey.com, **2015**.
[6] C. Sealy, *Mater. Today* **2008**, *11*, 65 – 68.
[7] F. Jaouen, J. Herranz, M. Lefèvre, J.-P. Dodelet, U. I. Kramm, I. Herrmann, P. Bogdanoff, J. Maruyama, T. Nagaoka, A. Garsuch, *ACS Appl. Mater. Interfaces* **2009**, *1*, 1623 – 1639.
[8] X. Ge, A. Sumboja, D. Wuu, T. An, B. Li, F. W. T. Goh, T. S. A. Hor, Y. Zong, Z. Liu, *ACS Catal.* **2015**, *5*, 4643 – 4667.
[9] M. P. Hyman, J. W. Medlin in *Catalysis, Vol 20*, RSC, **2007**, pp. 309 – 337.
[10] P. Hernandez-Fernandez, F. Masini, D. N. McCarthy, C. E. Strebel, D. Friebel, D. Deiana, P. Malacrida, A. Nierhoff, A. Bodin, A. M. Wise, *Nat. Chem.* **2014**, *6*, 732 – 738.
[11] M. S. El-Deab, T. Ohsaka, *Angew. Chem. Int. Ed.* **2006**, *45*, 5963 – 5966; *Angew. Chem.* **2006**, *118*, 6109 – 6112.
[12] J. Suntivich, H. A. Gasteiger, N. Yabuuchi, H. Nakanishi, J. B. Goodenough, Y. Shao-Horn, *Nat. Chem.* **2011**, *3*, 546 – 550.
[13] L. Dai, Y. Xue, L. Qu, H.-J. Choi, J.-B. Baek, *Chem. Rev.* **2015**, *115*, 4823 – 4892.
[14] S. Chen, J. Bi, Y. Zhao, L. Yang, C. Zhang, Y. Ma, Q. Wu, X. Wang, Z. Hu, *Adv. Mater.* **2012**, *24*, 5593 – 5597.
[15] N. Daems, X. Sheng, I. F. J. Vankelecom, P. P. Pescarmona, *J. Mater. Chem. A* **2014**, *2*, 4085 – 4110.
[16] H.-W. Liang, X. Zhuang, S. Brüller, X. Feng, K. Müllen, *Nat. Commun.* **2014**, *5*, 4973.
[17] Y. Meng, D. Voiry, A. Goswami, X. Zou, X. Huang, M. Chhowalla, Z. Liu, T. Asefa, *J. Am. Chem. Soc.* **2014**, *136*, 13554 – 13557.
[18] W. Zhang, Z.-Y. Wu, H.-L. Jiang, S.-H. Yu, *J. Am. Chem. Soc.* **2014**, *136*, 14385 – 14388.
[19] M. Levey, *J. Chem. Educ.* **1955**, *32*, 356 – 359.
[20] L. L. Zhang, X. S. Zhao, *Chem. Soc. Rev.* **2009**, *38*, 2520 – 2531.
[21] V. Etacheri, R. Marom, R. Elazari, G. Salitra, D. Aurbach, *Energy Environ. Sci.* **2011**, *4*, 3243 – 3262.
[22] V. R. Calderone, N. R. Shiju, D. Curulla Ferré, S. Chambrey, A. Khodakov, A. Rose, J. Thiessen, A. Jess, G. Rothenberg, *Angew. Chem. Int. Ed.* **2013**, *52*, 4397 – 4401; *Angew. Chem.* **2013**, *125*, 4493 – 4497.

[23] V. R. Calderone, N. R. Shiju, D. Curulla Ferré, A. Rose, J. Thiessen, A. Jess, E. van der Roest, B. Wiewel, G. Rothenberg, *Top. Catal.* **2014**, *57*, 1419 – 1424.
[24] Y. Tomita, K. Ueno, *Bull. Chem. Soc. Jpn.* **1963**, *36*, 1069 – 1073.
[25] JCPDS, Cards 45 – 0946 (MgO), 41 – 1487 (graphite).
[26] T. Miyazaki, T. Oshida, T. Nakatsuka, H. Yamamoto, M. Okamoto, M. Endo, *Mol. Cryst. Liq. Cryst.* **2002**, *388*, 85 – 90.
[27] L. Shi, H. Lin, K. Bao, J. Cao, Y. Qian, *Nanoscale Res. Lett.* **2010**, *5*, 20 – 24.
[28] G. Yang, H. Han, T. Li, C. Du, *Carbon* **2012**, *50*, 3753 – 3765.
[29] M. H. Rümmeli, C. Kramberger, A. Grüneis, P. Ayala, T. Gemming, B. Büchner, T. Pichler, *Chem. Mater.* **2007**, *19*, 4105 – 4107.
[30] M. H. Rümmeli, A. Bachmatiuk, A. Scott, F. Börrnert, J. H. Warner, V. Hoffman, J.-H. Lin, G. Cuniberti, B. Büchner, *ACS Nano* **2010**, *4*, 4206 – 4210.
[31] T. Tsumura, A. Arikawa, T. Kinumoto, Y. Arai, T. Morishita, H. Orikasa, M. Inagaki, M. Toyoda, *Mater. Chem. Phys.* **2014**, *147*, 1175 – 1182.
[32] T. Morishita, Y. Soneda, T. Tsumura, M. Inagaki, *Carbon* **2006**, *44*, 2360 – 2367.
[33] M. C. Mittelmeijer-Hazeleger, Understanding Adsorption in Micropores: A Study of Carbons, Soils and Zeolites, PhD thesis, University of Amsterdam, **2006**.
[34] M. Sevilla, A. B. Fuertes, *J. Mater. Chem. A* **2013**, *1*, 13738.
[35] S. Maldonado, K. J. Stevenson, *J. Phys. Chem. B* **2005**, *109*, 4707 – 4716.
[36] S. Kundu, T. C. Nagaiah, W. Xia, Y. Wang, S. V. Dommele, J. H. Bitter, M. Santa, G. Grundmeier, M. Bron, W. Schuhmann, *J. Phys. Chem. C* **2009**, *113*, 14302 – 14310.
[37] D. Deng, X. Pan, L. Yu, Y. Cui, Y. Jiang, J. Qi, W.-X. Li, Q. Fu, X. Ma, Q. Xue, *Chem. Mater.* **2011**, *23*, 1188 – 1193.
[38] L. Yu, X. Pan, X. Cao, P. Hu, X. Bao, *J. Catal.* **2011**, *282*, 183 – 190.
[39] A. J. Bard, L. R. Faulkner, *Electrochemical Methods: Fundamentals and Applications*, John Wiley & Sons, **2001**.
[40] P.-C. Li, C.-C. Hu, H. Noda, H. Habazaki, *J. Power Sources* **2015**, *298*, 102 – 113.

Received: November 13, 2015
Published online on December 4, 2015